Journal of Power Sources 208 (2012) 383–390

Contents lists available at SciVerse ScienceDirect

Journal of Power Sources

journal homepage: www.elsevier.com/locate/jpowsour

Numerical simulation of gas diffusion effects on charge/discharge characteristics of a solid oxide redox flow battery

Hiroko Ohmori [a,*], Syoichi Uratani [a], Hiroshi Iwai [b]

[a] Device & System Technology R&D Laboratories, Konica Minolta Technology Center, Inc., Takatsuki city, Osaka 569-8503, Japan
[b] Department of Aeronautics and Astronautics, Kyoto University, Sakyo-ku, Kyoto 606-8501, Japan

ARTICLE INFO

Article history:
Received 28 December 2011
Received in revised form 30 January 2012
Accepted 15 February 2012
Available online 23 February 2012

Keywords:
Rechargeable battery
Solid oxide electrochemical cell
Redox metal
Gas-diffusion based time-dependent 1-D simulation

ABSTRACT

Fundamental characteristics of a solid oxide redox flow battery consisting of solid oxide electrochemical cell (SOEC) and redox metal were studied by a gas-diffusion based time-dependent 1-D numerical simulation taking both the electrochemical and redox reactions into account. Close attention was paid to the distributions of the participating gas species and their effects on the charge/discharge performance. The volume expansion/reduction of the porous metal associated with the redox reaction was modeled as decrease/increase in local porosity. The numerical results for charge/discharge operation qualitatively showed the time-dependent distributions of the related physical quantities such as the gas concentrations, the active reaction region in the redox metal, and its local porosity. It was found that, to ensure effective redox reaction throughout the operation, the gas diffusion in the redox metal should be carefully designed.

1. Introduction

Development of a large-capacity energy-storage device is a key to realize an efficient smart grid system. It will enhance the capability of the smart grid to control and optimize the balance of power generation and consumption. It is also expected to function as a buffer for the fluctuation of power supply from the renewable energy sources [1–3]. Various types of energy storage are in use or under development today, in order to meet the requirement of the smart grid, that is, high rate capacity, high round-trip efficiency, long cycle life, and low life-cycle cost. For example, Na–S battery and Li-ion battery stand out for their steady charge/discharge characteristics. Low energy density, short shelf life, and use of toxic materials are, however, the drawbacks that must be overcome before a wide commercialization [4].

A solid oxide fuel cell is a device that directly converts the chemical energy of reactants into electricity, and has an advantage of high power generation efficiency. Recently much attention is also paid to its reverse reaction, electrolysis [5–7]. Because of the high potential of a solid oxide electrochemical cell (SOEC) as an energy conversion device, a new concept of storage battery was recently reported by Xu et al. [8]. This new concept battery consists of SOEC and redox metal. They experimentally investigated the storage-capacity, rate-capacity and round-trip efficiency to find its high potential to meet the demands of the smart grid. In this new battery, two reactions simultaneously proceed at two different locations. The electrochemical reaction occurs at the SOEC and the redox reaction at the redox metal. In the discharge operation, hydrogen is consumed at the SOEC to generate electricity and steam. The generated steam is supplied for the metal oxidation where hydrogen is produced and it is supplied to the SOEC for further electricity generation. Then in the charge operation, steam is consumed by the electrolysis operation at the SOEC to generate hydrogen. The hydrogen is used to reduce the metal oxide and the produced steam is supplied to the SOEC for further electrolysis. Hydrogen/steam mixture gas plays a key role as a carrier of oxygen atoms connecting two simultaneous reactions in both charge and discharge operations. Because the reaction rates are affected by the local concentrations of the participating species, to understand the fundamental transport phenomena in the system and their effects on the battery performance is essentially important.

The main objective of this study is to reveal the fundamental characteristics of a battery based on this new principle with our focus on the distributions of the participating gas species in the system and their effects on the performance. As a first step, we perform a gas-diffusion based time-dependent 1-D numerical simulation for one of the simplest battery configurations taking both the electrochemical and redox reactions into account. Time dependent charge/discharge performance, distributions of the concentrations and reaction rates and volume change effect of the redox metal are discussed.

* Corresponding author. Tel.: +81 72 6856159; fax: +81 72 6856129.
E-mail address: hiroko.ohmori@konicaminolta.jp (H. Ohmori).

0378-7753/$ – see front matter © 2012 Elsevier B.V. All rights reserved.
doi:10.1016/j.jpowsour.2012.02.054

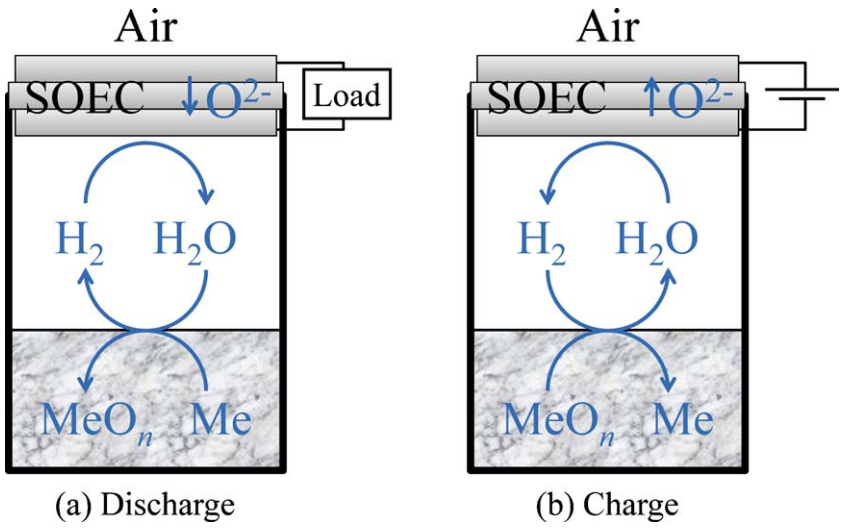

Fig. 1. Reactions (a) in discharge operation and (b) in charge operation.

2. Numerical procedure

2.1. Outline of battery

The concept of the battery is schematically explained in Fig. 1 with the reactions occurring at different positions. It is made of two major components, a planar SOEC and the redox metal facing to the SOEC. The redox metal is typically made of fine metal particles and is symbolized as Me. In discharge operation shown in Fig. 1(a), two electrochemical reactions and oxidation of Me by steam proceed simultaneously in the system. The SOEC works as a fuel cell in this mode. Oxide ion, O^{2-}, is formed on the air-side electrode through the electrochemical reaction expressed as:

$$1/2(O_2) + 2e^- \rightarrow O^{2-} \quad (1)$$

O^{2-} migrates inside the electrolyte to the other side of the SOEC and reacts electrochemically with hydrogen as:

$$H_2 + O^{2-} \rightarrow H_2O + 2e^- \quad (2)$$

The generated steam is transported to the redox metal by gas diffusion. It oxidizes the redox metal into metal oxide as:

$$Me + nH_2O \rightarrow MeO_n + nH_2 \quad (3)$$

This reaction generates hydrogen that diffuses to the SOEC electrode and is consumed as fuel for the power generation. With reactions (1)–(3) combined, the total reaction can be written as below:

$$Me + n/2(O_2) \rightarrow MeO_n \quad (4)$$

When all (or some part of) the redox metal is oxidized, the battery needs to be recharged. In the charge operation shown in Fig. 1(b), all the above reactions proceed in reverse directions. The SOEC works as an electrolyser in this mode. The electrochemical reactions on the air-side and hydrogen-side electrodes are expressed as below, respectively:

$$O^{2-} \rightarrow 1/2(O_2) + 2e^- \quad (5)$$

$$H_2O + 2e^- \rightarrow H_2 + O^{2-} \quad (6)$$

The hydrogen generated on the hydrogen-side electrode is transported to the redox metal by gas diffusion. It reduces the metal oxide as:

$$MeO_n + nH_2 \rightarrow Me + nH_2O \quad (7)$$

From the reactions (5)–(7), the total reaction in charge operation can be described as below:

$$MeO_n \rightarrow Me + n/2(O_2) \quad (8)$$

When all (or some part of) the redox metal is reduced, the charge operation is completed and the system is ready for next discharge.

The overall reaction equations express by Eqs. (4) and (8) are similar to that of a metal–air battery. There are, however, clear differences that distinguish the new battery from the metal–air battery. It applies oxygen ion conductive material as an electrolyte. O^{2-} transfer operation involves more electrons thus it achieves higher storage-capacity at a higher rate. Use of hydrogen/steam mixed gas is also a unique advantage if we consider that hydrogen/steam gas transfer is much easier than metal ion transfer. Furthermore in the new battery, the electrochemical reaction (the SOEC) is physically separated from the redox reaction (the redox metal). The separation of the redox metal from other parts prevents structural damages that may be caused by volume change of the redox metal associated with redox reaction. To bridge the electrochemical reaction and the redox reaction occurring at different positions, hydrogen/steam mixture gas is needed between the SOEC and the redox metal. The steam works as an oxygen-atom carrier between the SOEC and the redox metal. The required amount of the mixture gas is small because hydrogen atom is recycled during the oxygen-atom transfer in a form of steam.

The direction of the reversible redox reaction is governed by the mixture gas composition in the container. When hydrogen partial pressure is above the equilibrium pressure of redox reaction at a certain temperature, reduction is dominant, and vice versa. If there is no current at the SOEC, the mixture gas composition reaches to the equilibrium state and the redox reaction apparently stops in the container. On the other hand, if there is a certain amount of charge/discharge current at the SOEC associated with the electrochemical reactions, the gas composition in the container changes and it immediately leads the redox reaction into proceeding in a corresponding direction. Under quasi-steady condition, the amount of hydrogen reacting at the SOEC is the same as that of hydrogen reacting at the redox metal, except when one of the coupled reactions is too fast or too slow.

Redox material is typically small metal particles to ensure a large surface area. As a bulk material, we treat it as porous material in this study. When the redox metal is oxidized, its volume increases resulting in a reduction of the pore space where the gas species

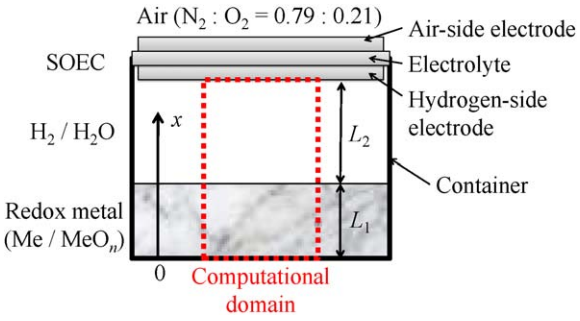

Fig. 2. A schematic figure of the battery including the SOEC and the redox metal.

diffuse. The change of the condition of porous material affects gas diffusion and redox reaction rate.

In this study we choose iron as the redox metal. Steam oxidizes Fe into Fe_3O_4 as below [9–11]:

$$3Fe + 4H_2O \underset{\text{charge}}{\overset{\text{discharge}}{\rightleftarrows}} Fe_3O_4 + 4H_2 \tag{9}$$

The energy stored in iron corresponds to the Gibbs free energy change of reactions (1) and (2). The theoretical energy density is estimated to be 1323 Wh (kg-Fe)$^{-1}$ Fe with hydrogen reacting at 600 °C, and charge capacity density 1280 Ah (kg-Fe)$^{-1}$.

As explained above, the separation of power generation part and power storage part is one of the key points of this battery. It also gives us freedom to independently design the size of the SOEC and the amount of the redox metal. As metal particles can easily be filled in various shapes, both tubular and planar SOEC are available for this battery.

2.2. Battery design and computational domain

We assume one of the simplest battery configurations. As schematically shown in Fig. 2, it consists of the planar SOEC, the redox metal and a container. The air-side electrode of the SOEC is exposed to the air (N_2:O_2 = 0.79:0.21) while the hydrogen-side electrode is to the hydrogen/steam mixture gas in the container. The total pressure inside the container is assumed to be 1 atm. The redox metal is placed inside the container. Note that, unlike the flow-type configuration in Xu et al. [8], there is no bulk fluid motion in the container in this study. Focusing on the center part of the system marked as a computational domain in Fig. 2, we assume one-dimensional phenomena in the x-direction neglecting the sidewall effects. The main design parameters of the system are the length of the redox metal, L_1, and the distance between the SOEC and the redox metal, L_2. L_2 is kept constant at 1 cm throughout this study. L_1 is related to the amount of the redox metal per unit area of the SOEC electrode. As a standard condition, we place 1 g cm^{-2} of reduced metal with a porosity of 0.7 which results in L_1 of 4.2 mm. We assume L_1 is constant during the operation unless the amount of the redox metal is varied. As the redox metal is iron, its volume increases by a factor of 2.1 when it is oxidized. The volume expansion/reduction caused by redox reaction affects the local porosity of the redox metal.

2.3. Numerical modeling

In this paper, the distributions of the participating gas species in the system and their effects on the battery performance are major interests. 1-Dimensional numerical simulation based on a mass diffusion equation is conducted to examine the dynamic behavior of the battery affected by interaction of two parallel reactions.

2.3.1. Governing equation

The governing equation is the time-dependent 1-D diffusion equation:

$$\frac{\partial C_j}{\partial t} = \frac{\partial}{\partial x}\left(D\frac{\partial C_j}{\partial x}\right) + S_j \tag{10}$$

C, D, S and j denote the concentration of hydrogen or steam, gas diffusion coefficient, mass production/consumption and species, respectively. Mass production/consumption is associated with the metal redox reaction. As explained in the latter sections, we assume the concentration overpotential in the SOEC electrodes is negligible. The mass production/consumption is expressed as boundary conditions on the SOEC side. On the other hand for the redox metal, we consider the diffusion inside the porous material thus the mass production/consumption effect appears in the equation as a source term.

Inside the porous material, gas diffusion is limited and its effect is taken into account by considering an effective diffusion coefficient, D_{eff}. A precise evaluation of D_{eff} is a challenging problem itself as it depends on the microstructure of the porous material. As this study is a first step to understand the fundamental characteristics of the new battery, we treat it in a simple way as:

$$D_{\text{eff}} = D\frac{\varepsilon}{\tau} \tag{11}$$

where ε and τ are the porosity and tortuosity factor of the porous material. Following Melkote and Jensen [12], the tortuosity factor is assumed to be reciprocal of the porosity, $\tau = 1/\varepsilon$. We further assume that the representative pore diameter is much longer than the mean free path of hydrogen and neglect Knudsen diffusion (rarefaction effect).

2.3.2. Metal redox reaction model

We assume local thermal equilibrium and a large effective thermal conductivity of the porous material resulting in a uniform temperature assumption for the porous part. In a real system, its temperature is to be determined as a result of the balance of the heat generation/absorption in the system and heat loss to surroundings. For simplicity, in this study, we set a constant temperature of 400 °C.

We performed preliminary in-house experiment using iron particles at 400 °C and obtained volume specific reaction rate. It is expressed in terms of the partial pressures of hydrogen and steam, p_{H2} and p_{H_2O}. When hydrogen partial pressure is below the equilibrium pressure, the hydrogen generation rate is calculated as:

$$S = \{-(k_1 \times p_{H_2}) + (k_2 \times p_{H_2O})\} \times M \tag{12}$$

and is applied to Eq. (10). k_1 and k_2 are reaction coefficients determined from the experiments while M is the molar density of the reactant. When hydrogen partial pressure is above the equilibrium pressure, the hydrogen consumption rate of the redox metal is calculated by the same equation with the figure minus.

2.3.3. Electrochemical model of the SOEC

The SOEC was assumed to have uniform temperature of 600 °C and work under uniform current density condition. Electromotive force (EMF), E, is evaluated by Nernst equation.

$$E = E^0 + \frac{RT}{2F}\ln\left(\frac{p_{H_2} \times p_{O_2}^{1/2}}{p_{H_2O}}\right) \tag{13}$$

$$E^0 = -\frac{\Delta G^0}{2F} \tag{14}$$

Here, E^0, R, T, F and P are standard electromotive force, universal gas constant, temperature, Faraday constant and partial pressure,

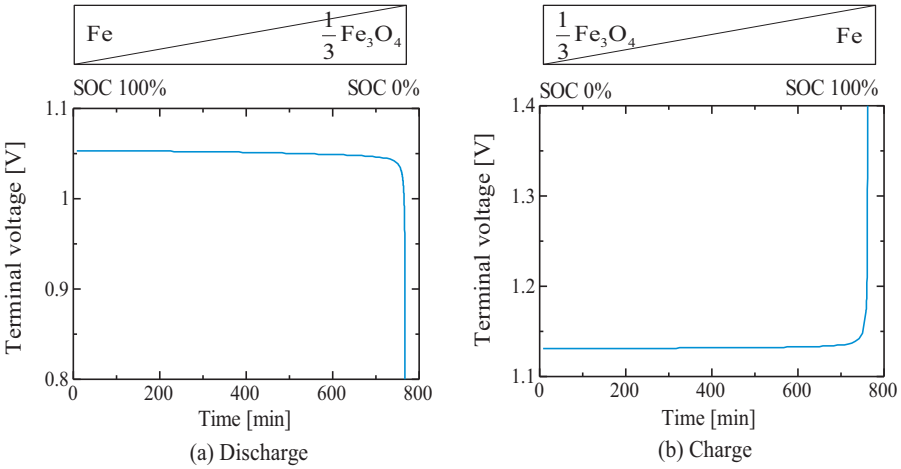

Fig. 3. Time history of terminal voltage (a) in charge operation and (b) discharge operation at 100 mA cm^{-2} with 1 g-Fe cm^{-2}.

respectively. Concentration overpotential was neglected assuming thin electrodes. The area specific resistances, ASR, associated with IR loss and the activation overpotential were set as 1e−5 and 2.5e−5 [Ω m^2], respectively, by fitting *i*–*V* curve of an experiment at 600 °C [13]. Although the activation overpotential in electrolysis mode is generally different from that of fuel cell mode, the same expression was assumed in this study for simplicity. IR loss, η_{ohm}, and activation overpotential, η_{act}, are expressed as:

$$\eta_{ohm} = \mathrm{ASR}_{ohm} \times i \tag{15}$$

$$\eta_{act} = \mathrm{ASR}_{act} \times i \tag{16}$$

where *i* is the current density (absolute value). Then the terminal voltage, *V*, can be obtained as:

$$\text{Discharge}: \ V_{discharge} = E - (\eta_{ohm} + \eta_{act}) \tag{17}$$

$$\text{Charge}: \ V_{charge} = E + (\eta_{ohm} + \eta_{act}) \tag{18}$$

for the discharge operation and charge operation, respectively.

2.3.4. Numerical procedure

An in-house program code was developed and was applied to the battery model shown in Fig. 2. The governing equations were discretized using the finite volume method. Non-uniform grid system was applied with finer grid spacing in the redox metal porous medium where a steep concentration gradient was expected. A systematic grid test was conducted to confirm that results had no grid dependency.

2.3.5. Computational conditions

The steam/hydrogen mixture in the container is initially at equilibrium state at 600 °C. The redox metal is totally reduced at the beginning of the discharge operation, while it is totally oxidized at the beginning of the charge operation. We assume the temperature of the SOEC and the mixture gas is constant at 600 °C while the redox material operates at 400 °C. The average current density of the SOEC and the amount of the redox metal in the container are basically set at 100 mA cm^{-2} and 1 g cm^{-2}, respectively. They are varied only in Sections 3.4 and 3.5 to see their effects on the operation.

3. Results and discussion

3.1. Fundamental characteristics under charge/discharge operations

The fundamental characteristics of the battery are discussed taking the case of the current density at 100 mA cm^{-2}. Fig. 3 shows the time history of the terminal voltage under charge/discharge conditions. State of charge, SOC, is defined as the rate of electricity (Ah) stored in the battery to that of full charge. When the battery is fully charged, SOC is 100%. The terminal voltage under charge condition is naturally higher than that under discharge condition. Except for the last 10% of each operation, the redox reaction proceeds fast enough and it balances to the electrochemical reaction resulting in an almost constant terminal voltage. Under this condition, the system appears to be in a quasi-steady state. A marked rise of the terminal voltage in the charge operation at SOC larger than 90% reflects a rise of hydrogen partial pressure in the container. It is caused by limited consumption of hydrogen at the redox metal corresponding to Eq. (7). On the other hand, a marked decline of the terminal voltage in the discharge operation at SOC smaller than 10% reflects a decline of hydrogen partial pressure in the container. It is caused by limited generation of hydrogen at the redox metal corresponding to Eq. (3).

3.2. Gas diffusion during operation

Fig. 4 shows the distribution of hydrogen partial pressure inside the container, corresponding to Fig. 3. The area of $0.0 < x < 4.2$ mm corresponds to the porous part with the redox metal, and the SOEC electrode surface is located at $x = 14.2$ mm. As the mixture gas is binary, steam partial pressure can easily be calculated from Fig. 4. Under discharge operation, the hydrogen generated by metal oxidation diffuses to the SOEC while hydrogen diffuses in the opposite direction under charge operation. The figure shows that the partial pressure of hydrogen in the container generally takes a high value when SOC is high. Its increase/decrease during the charge/discharge process is consistent with the marked rise/decline of the terminal voltage observed in Fig. 3. It also shows that the distribution is relatively flat in *x*-direction in particular under charge operation. In both discharge/charge operations, the distribution is almost linear in the area of $4.2 < x < 14.2$ mm. Inside the porous part, on the other hand, the gradient is not constant and generally larger reflecting the limited diffusion coefficient express by Eq. (11). The non-linear distribution pattern gradually changes as SOC

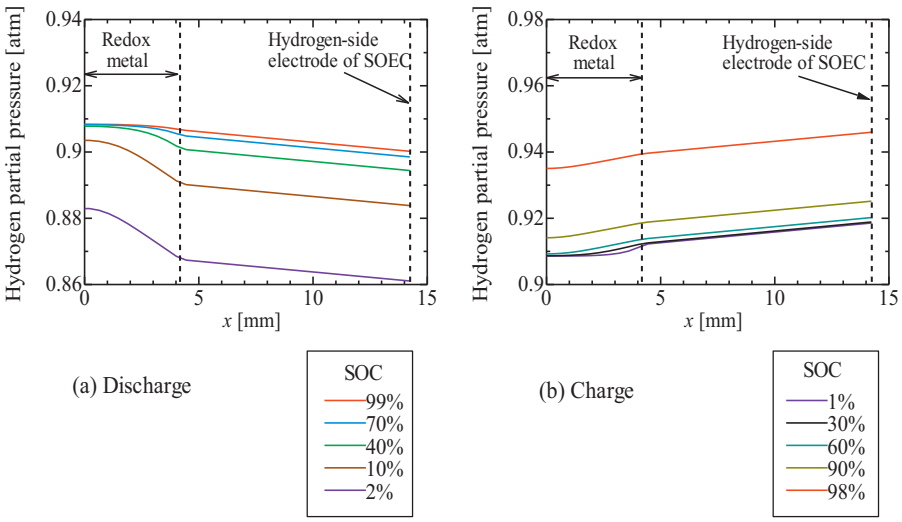

Fig. 4. Distribution of hydrogen partial pressure in the container (a) in discharge operation and (b) in charge operation.

increases/decreases. The increase of the gradient is more prominent in the discharge operation.

3.3. Evolution of redox reaction area

Partial pressure distribution in the porous part is affected by the generation/consumption of hydrogen and steam associated with the metal redox reaction. The distribution of hydrogen-generation rate is shown in Fig. 5. Negative value in Fig. 5(b) corresponds to the hydrogen consumption during the charge operation. As explained in the Section 2.3.5, it is assumed that the redox metal, iron, is completely reduced at the initial state of the discharge operation and is completely oxidized at the initial state of the charge operation. Therefore the increase of SOC in charge operation and the decrease of that in discharge operation correspond to the elapsed time.

During the discharge operation, steam generated at the SOEC approaches to the redox metal by diffusion. Oxidation of the metal first proceeds actively near the surface region close to the SOEC (right side in Fig. 5(a)) due to relatively high steam partial pressure. As oxidation goes on, the portion of the metal oxide increases near the surface region and the active reaction region gradually shifts into the inner part where fresh reduced metal exists. The increase of the metal oxide can be confirmed in Fig. 6, which shows the distribution of Fe_3O_4 ratio in the redox metal region. It is worth noting in Fig. 6(a) that approximately 30% of metal near $x = 0$ is still not oxidized at SOC = 10% in discharge operation. It is expected that the drastic decrease of the terminal voltage at SOC < 10% observed in Fig. 3(a) can be delayed by improving the gas diffusion in the redox metal. Similar shift of the active reaction region can be seen during charge operation as shown in Figs. 5(b) and 6(b).

Fig. 7 shows the distribution of local porosity in the redox metal. Because the particles expand in volume when they are oxidized, the local porosity changes depending on the degree of oxidation. At the initial state, it distributes uniformly in both discharge/charge operations. Its value is noticeably low for the charge operation because the particles are fully oxidized at the initial state. When the portion of the oxidized particle is large, local porosity is low and the effective diffusion coefficient takes a small value. The effect of the particle expansion can be clearly seen in Figs. 4 and 5. In discharge operation shown in Fig. 5(a), the reaction rate at the inner region is moderate even at the beginning due to moderate diffusion through the pores. In the charge operation shown in Fig. 5(b), on the other hand, the reaction rate is close to zero around the inner region at the beginning of operation because of insufficient diffusion limited by the expanded particles. In Fig. 4(a), a steep partial pressure gradient is formed near the surface region, $x = 4.2$, and it gradually expands to inner region, which agree well with the shift of the active reaction region seen in Fig. 5(a). Under the calculation condition set in this study, the gas diffusion is not completely blocked by the expanded particles (metal oxide). It should be noted, however, that inappropriate filling of the particles may cause a sever decrease of the gas diffusion coefficient to cause a fatal delay of the redox reaction.

Concerning the diffusion in the space between the SOEC and the redox metal, no practical problem is observed under the calculation conditions and geometry set in this study. Diffusion inside the porous redox metal is the major mass transfer phenomenon that needs to be carefully considered.

3.4. Effects of current density

Fig. 8 shows the effects of the current density on the battery operation. In discharge operation, the current density was varied in the range between 10 and 2000 mA cm^{-2} and was kept constant during each operation. All other conditions were unchanged from the base condition discussed above. A high current density means the enhanced electrochemical reaction on the SOEC. The terminal voltage is generally low at a high current density condition, mainly because of the large ohmic and activation losses. The terminal voltage, or more precisely the EMF, is also affected by the hydrogen/steam composition at the electrode surface of the SOEC. When the current density is raised, partial pressure of steam increases. It enhances the hydrogen generation on the redox metal until the hydrogen generation and consumption balances. If two reactions balance, a quasi-steady state is established and the power generation continues at a certain EMF corresponding to the gas composition achieved. As SOC decreases in proportion to the increase of the elapsed time, the amount of fresh reduced metal available for the hydrogen generation decreases. As Fig. 8(a) clearly shows, the terminal voltage sharply decreases at a certain SOC in each current density. Under this SOC, high steam partial pressure is needed to enhance the metal oxidation reaction but it inevitably leads a sharp drop of EMF resulting in an insufficient operation of the battery. The sharp drop of the terminal voltage (EMF) is observed at a lower SOC for a higher current density.

The key phenomena in charge operation are the same as those in discharge operation discussed above, except for the opposite direction of the reactions. One noticeable difference is that the current density set in the calculations is low compared to that of discharge

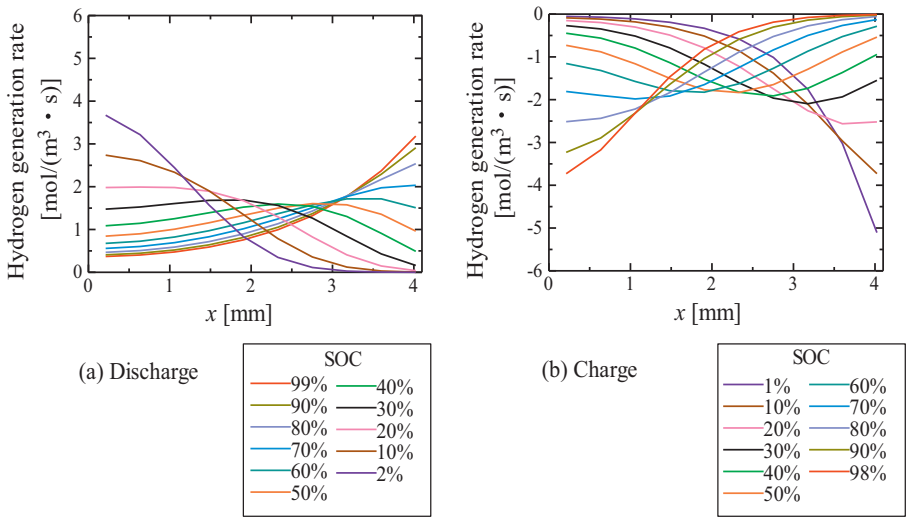

Fig. 5. Distribution of hydrogen generation rate in the redox metal region (a) in discharge operation and (b) in charge operation.

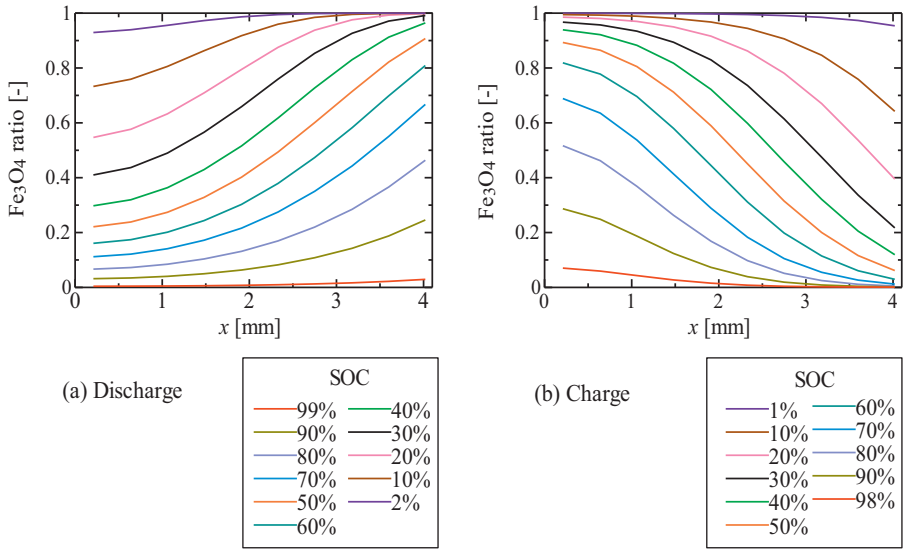

Fig. 6. Distribution of Fe_3O_4 ratio in the redox metal region (a) in discharge operation and (b) in charge operation.

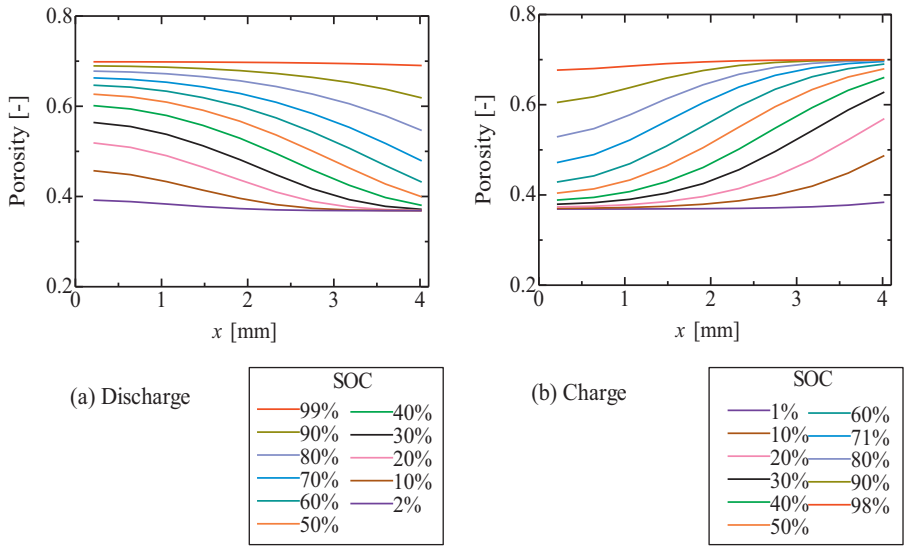

Fig. 7. Distribution of porosity of the redox metal region (a) in discharge operation and (b) in charge operation.

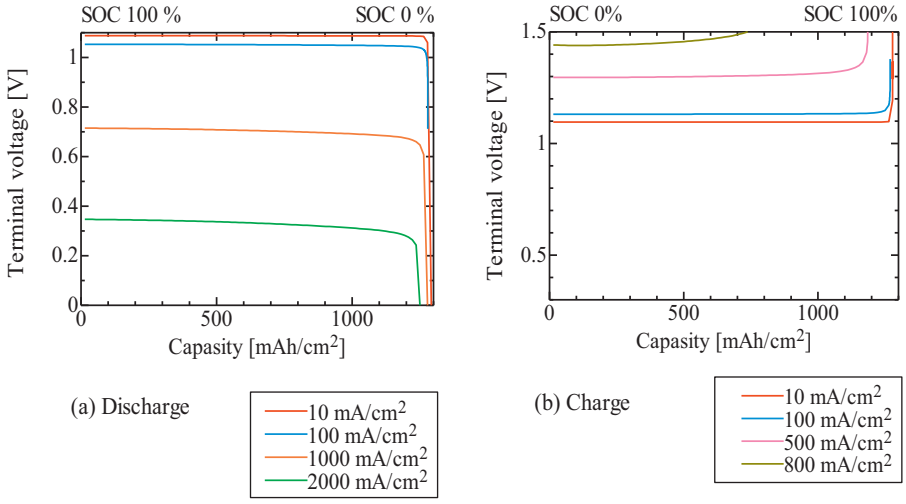

Fig. 8. Effects of the current density on the terminal voltage with 1 g-Fe cm^{-2} (a) in discharge operation and (b) in charge operation.

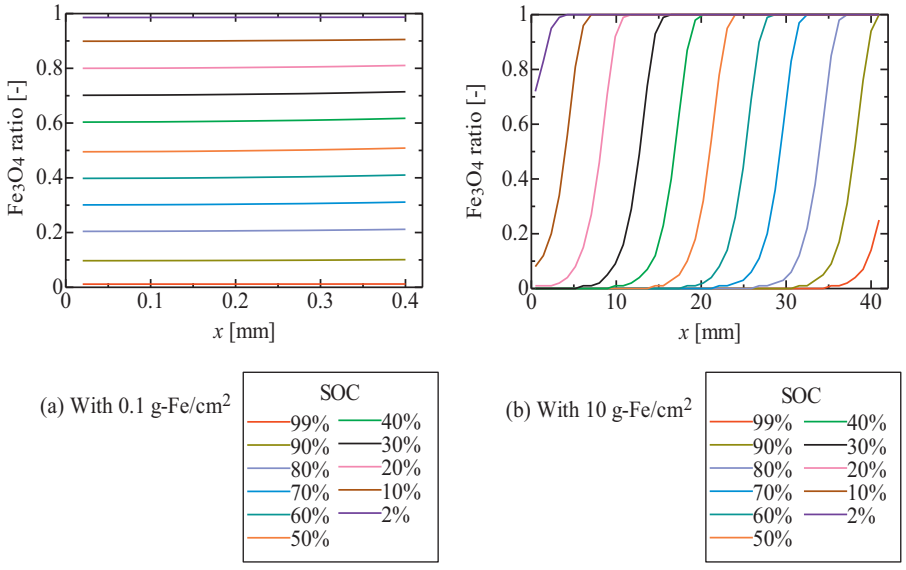

Fig. 9. Effects of the amount of the redox metal on distribution of Fe_3O_4 ratio in discharge operation at 100 mA cm^{-2} (a) with 0.1 g-Fe cm^{-2} and (b) 10 g-Fe cm^{-2}.

operation. To avoid a rapid degradation of the SOEC electrodes, the terminal voltage in charge operation should not be raised too high.

3.5. Amount of the redox metal

From the battery concept, it is clear that the battery capacity is determined by the total amount of the redox metal in the system while the reaction rates are primarily controlled by the current density of the SOEC. Therefore the amount of the redox metal per unit surface area of the SOEC electrode is an important design parameter of the battery. Calculations were conducted varying the amount of the redox metal in the container. Fig. 9 shows the distribution of Fe_3O_4 ratio in discharge operation. Note that in Fig. 9(a) and (b), the amount of the redox metal was set 0.1 g cm^{-2} and 10 g cm^{-2}, respectively. In this calculation, the initial porosity of reduced metal was unchanged from the standard condition, 0.7. Variation of the redox metal amount also means that the length of the redox metal part, L_1, is varied. In Fig. 9(a), the metal oxidation proceeds almost uniformly. It is ideal from the reaction point of view, because all the redox metal is effectively utilized. The low battery capacity, however, is an obvious penalty as a system. The case with 10 g cm^{-2}, the redox metal has a large battery capacity but as shown in Fig. 9(b) a significant delay of the redox reaction is observed at the inner part. This result shows that setting a suitable amount of the redox metal is a key to design this battery.

4. Conclusions

To understand the fundamental characteristics of a solid oxide redox flow battery, a gas-diffusion based time-dependent 1-D numerical simulation was conducted taking both the electrochemical and redox reactions into account. The electrochemical reaction rate at the SOEC is controlled by setting the current density as a boundary condition. Volume change of the redox metal is modeled as the change of local porosity and its effects on the gas diffusion is considered. Particular attention is paid to the distributions of the participating gas species, reaction rate, SOC and porosity in the porous redox metal. The following conclusions are obtained:

(1) Fundamental charge/discharge behavior of a solid oxide redox flow battery is numerically predicted. Reasonable and

consistent results are obtained to discuss fundamental characteristics of the battery qualitatively.

(2) The balance of reaction rates between the metal redox reaction and the electrochemical reaction is an important factor. When two reactions equally proceed, the terminal voltage is almost constant and the system appears to be in a quasi-steady state. Under a condition in which the metal redox reaction becomes slow, the gas composition in the container shifts in a direction to lower the system performance. Because of this slow reaction, the terminal voltage quickly increases/decreases at the end of the charge/discharge operation.

(3) The gas diffusion in the redox metal needs to be carefully designed to ensure an effective reaction throughout the operation. At the beginning of the charge/discharge operation, the redox reaction is active near the surface region of the redox metal. The active region gradually moves to the inner region. The volume change of the redox metal affects the effective diffusion coefficient and its effect is particularly important in discharge operation. The volume of the redox metal expands during the discharge operation leading reduction of the effective diffusion coefficient which limits the effective metal redox reaction.

References

[1] J.A. Turner, Science 285 (1999) 687–689.
[2] M. Roeb, H. Muller-Steinhagen, Science 329 (2010) 773–774.
[3] N.S. Lewis, Science 315 (2007) 798.
[4] Z. Yang, J. Zhang, M.C.W. Kintner-Meyer, X. Lu, D. Choi, J.P. Lemmon, J. Liu, Chem. Rev. 111 (2011) 3577–3613.
[5] A. Hauch, S.D. Ebbesen, S.H. Jensen, M. Mogensen, J. Electrochem. Soc. 155 (2008) B1184–B1193.
[6] K. Eguchi, T. Hatagishi, H. Arai, Solid State Ionics 86–88 (1996) 1245–1249.
[7] T. Ishihara, T. Kanno, ISIJ Int. 50 (2010) 1291–1295.
[8] N. Xu, X. Li, X. Zhao, J.B. Goodenough, K. Huang, Energy Environ. Sci. 4 (2011) 4942–4946.
[9] K. Otsuka, C. Yamada, T. Kaburagi, S. Takenaka, Int. J. Hydrogen Energy 28 (2003) 335–342.
[10] E. Lorente, J.A. Pena, J. Herguido, Int. J. Hydrogen Energy 33 (2008) 615–626.
[11] K. Otsuka, T. Kaburagi, C. Yamada, S. Takenaka, J. Power Sources 122 (2003) 111–121.
[12] R.R. Melkote, K.F. Jensen, AIChE J. 38 (1992) 56–66.
[13] T. Suzuki, Z. Hasan, Y. Funahashi, T. Yamaguchi, Y. Fujishiro, M. Awano, Science 325 (2009) 852–855.